Journal of Mathematical Modeling
Vol. -, No. -, 2026, pp. -. Research Article

JMM

Numerical simulation of nonlinear Galilei invariant advection–diffusion equations via fractal–fractional operators

Parisa Rahimkhani [a,∗], **Sedigheh Sabermahani** [b], **Thabet Abdeljawad** [c,∗]

[a]*Faculty of Science, Mahallat Institute of Higher Education, Mahallat, Iran*
[b]*Department of Mathematics Education, Farhangian University, P.O. Box 14665-889, Tehran, Iran*
[c]*Department of Fundamental Sciences, Faculty of Engineering and Architecture, Istanbul Gelisim University, Avcılar- Istanbul, 34310, Türkiye*

Email(s): rahimkhani.parisa@mahallat.ac.ir, s.saber@cfu.ac.ir, tabdeljawad@gelisim.edu.tr

Abstract. In this paper, a new class of fractal-fractional differential equations called the fractal-fractional Galilei invariant advection–diffusion equation is introduced for the first time. Then, we introduce a method based on the fractional Genocchi functions for solving this problem. To achieve the stated objective, we first derive the fractal-fractional and integer-order integral operators for the fractional Genocchi functions in the Atangana-Riemann-Liouville sense. Then, the obtained integral operators of the fractional Genocchi functions, along with certain properties of the fractional Genocchi functions, are utilized within a collocation method to reduce the fractal-fractional Galilei invariant advection- diffusion equation to a system of algebraic equations involving the unknown coefficients. Finally, the convergence analysis of the proposed method is examined in the Sobolev space. In addition, illustrative examples are provided to demonstrate the validity and applicability of the proposed method.

Keywords: Fractal-fractional nonlinear Galilei invariant advection-diffusion equations, fractional Genocchi functions, fractal-fractional integral operators, convergence analysis.
AMS Subject Classification 2010: 80M22, 28A80, 41A10.

1 Introduction

Fractional calculus, as an emerging and powerful branch of applied mathematics, has attracted growing attention due to its ability to model complex phenomena exhibiting memory and non-local behavior. Unlike classical integer-order derivatives and integrals, fractional operators incorporate historical dependence, making them well-suited for describing real-world systems in areas, namely viscoelasticity [45], control theory [44], fluid mechanics [18], diffusion [13], and electromagnetism [7]. Recently, there has been a significant advancement in the development of numerical approaches to solve

∗Corresponding author
Received: 05 February 2026/ Revised: 29 July 2026/ Accepted: 31 July 2026
DOI: 10.22124/jmm.2026.32909.2994

fractional differential equations (FDEs), including the fractional-order clique functions method to obtain solutions for the left-sided Bessel fractional integro-differential equations [30], the fractional-order generalized Chelyshkov wavelets strategy to efficiently address of nonlinear FDEs [23], the 2D Gegenbauer wavelets methodology for solving tempered fractional model of the nonlinear Klein–Gordon equation [35], the Hahn hybrid functions method to provide solutions to the distributed order fractional Black-Scholes European option pricing problem [31], the Chebyshev cardinal functions/wavelets method for the time fractional coupled Klein-Gordon-Schrödinger equations [14], the wavelets neural networks method for solving Ψ-fractional differential equations [27], the adaptive computational approaches for solving time-fractional parabolic problems involving delay in time [10], fractional reaction-subdiffusion equations [11], time-fractional semilinear advection-reaction-diffusion equations with variable coefficients [9], distributed order fractional differential equations [28], and distributed-order fractional optimal control problem [6].

Fractal-fractional (FF) calculus represents a novel and rapidly evolving domain within mathematical analysis, integrating the non-local, memory-dependent characteristics of fractional calculus with the geometric intricacies of fractal structures. This unified framework enables the effective modeling of dynamic systems that exhibit both hereditary effects and geometrical irregularities-phenomena frequently encountered in diverse fields such as dynamics of drilling system [3], convective fluid motion [2], simulation of the Ebola virus [42], chaotic different problem [4], etc. Over the past few years, significant attention has been devoted to the development of robust numerical schemes for the analysis and approximation of FF differential equations, for instance the alternative wavelets for variable-order FF differential equations systems with power and Mittag-Leffler kernels [32], the Legendre polynomials method for solving FF optimal control problems [12], the fractional shifted Morgan-Voyce neural networks method to solve FF pantograph differential equations [26], the meshless scheme based on the moving least squares shape functions for the nonlinear FF advection-diffusion equation [17], the generalized Lucas wavelet technique to solve nonlinear FF optimal control problems [38], the peridynamic method for solving two dimensional FF PDEs [36], and the 2D Chelyshkov polynomials method for the FF 2D Emden-Fowler equation [16].

The Galilei-invariant advection–diffusion equations (G-ID-DEs) play a fundamental role in modeling the evolution of a wide range of critical phenomena in engineering and the physical sciences [5]. Given their broad applicability and theoretical significance, a comprehensive investigation of these equations from diverse analytical and numerical perspectives is of paramount importance. In response to this necessity, a variety of advanced numerical techniques have been proposed and employed for their solution, including the Gegenbauer wavelets method [22], local meshless method [8], Vieta-Lucas functions method [15], operational matrix method [46], and Crank–Nicolson method [1].

The convergence analysis of numerical methods is a critical issue in scientific computing, as it ensures the reliability of the proposed numerical method and its capacity to accurately approximate the exact solution. In this direction, several recent studies have developed rigorous convergence analyses and adaptive numerical approaches for equidistribution, fractional-order systems, Robin or mixed boundary conditions, and singularly perturbed problems. For example, in [39], a rigorous convergence analysis on an adaptive mesh has been proved to guarantee uniform linear accuracy in time and uniform quadratic convergence in space for parameterized systems with mixed boundary conditions. In [40], the authors provided a rigorous convergence analysis, proving that the proposed adaptive discretization scheme achieves second-order parameter-uniform spatial convergence for singularly perturbed parabolic problems with Robin boundary conditions. Theoretical validation in [21] establishes second-order uniform convergence for a hybrid difference scheme applied to nonlinear singularly perturbed integral boundary value problems, supported by rigorous a priori and a posteriori error estimates. In [24], the authors introduced an iterative physics-informed neural network and provided a rigorous convergence analysis, proving that the empirical loss function remains bounded in the L^2 norm within the Barron space for singularly perturbed strongly coupled magnetohydrodynamic systems. In [19], a rigorous convergence analysis for a Schwarz waveform relaxation-type domain decomposition algorithm has been provided, guaranteeing uniformly convergent numerical approximations for singularly perturbed Gierer-Meinhardt systems featuring sharp spike components. In [20], a higher-order convergence analysis was carried out for singularly perturbed semilinear reaction–diffusion problems with mixed boundary conditions and nonsmooth data, which showed that suitably designed upwind–hybrid discretizations achieved nearly second-order uniform accuracy even in the presence of boundary and interior The authors established in [41] a rigorous higher-order convergence theory for graded-mesh $L1$ schemes applied to multi-term time-fractional integro-differential equations, provided sharp error bounds and uniform stability analysis, and demonstrated that the graded discretization effectively resolved the initial singular layer and significantly enhanced the convergence rate. In [37], the authors developed stability and convergence analysis of the $L1/L1-2$ Legendre spectral method for non-local weakly singular integro-PDEs.

The favorable characteristics of the FF derivative, as previously discussed, coupled with the absence of a corresponding FF formulation for the G-ID-DEs, provide strong motivation for the development of a novel FF-based representation of these equations. To effectively address the significant analytical and computational challenges posed by this new formulation, we further introduce a robust and efficient numerical scheme tailored to its solution. In what follows, we focus our investigation on the FF nonlinear G-ID-DEs in the following form:

$$V_t(x,t)+\rho V_x(x,t)=\iota\, {}^{ARL}D_t^{\nu,\eta}V_{xx}(x,t)+\mathscr{H}(x,t,V(x,t))+K(x,t), \tag{1}$$

$$V(x,0)=f(x), \quad V(0,t)=g_0(t), \quad V(1,t)=g_1(t), \tag{2}$$

where

$$0<\nu,\eta\leq 1, \qquad (x,t)\in(0,1)\times(0,1).$$

Here, $V(x,t)$ denotes the dependent variable-such as concentration or temperature-as a function of time t and spatial position x; ρ represents the velocity field, characterizing the advection or transport of V; ι denotes the diffusion coefficient, quantifying the rate at which diffusion occurs; and $\mathscr{H}$ and K denote nonlinear source terms, accounting for reactions or spatially distributed sources and sinks; $f(x), g_0(t)$ and $g_1(t)$ are continuous specific functions on the interval $[0,1]$ and ${}^{ARL}D_t^{\nu,\eta}$ is the FF derivative of order (ν,η) in the Atangana–Riemann–Liouville (ARL). Throughout this work, the exact solution is assumed to satisfy

$$V(x,t)\in L^2((0,1)\times(0,1)).$$

Moreover, the source term and initial-boundary data are assumed to satisfy

$$K(x,t)\in L^2((0,1)\times(0,1)), \quad f(x),\, g_0(t),\, g_1(t)\in L^2(0,1).$$

Under these assumptions, the proposed approximation method based on the fractional-order Genocchi functions is well defined.

To address the above problem, we apply a class of basis functions termed fractional Genocchi functions (FGFs). These functions are distinguished by the computational simplicity of their fractional and integer-order integrals and derivatives. Capitalizing on this advantageous property, we construct new operators, such as FF integral and integer-order integral operators. The proposed methodology involves employing the FGFs and the associated operators within a collocation framework to transform the original problem into a system of algebraic equations, thereby facilitating the determination of the unknown solution. To assess the accuracy and robustness of the developed scheme, a series of illustrative numerical examples are presented. The main contributions and innovative aspects of the proposed framework can be summarized as follows:

- **Introduction of a new FF Galilei-invariant model:** A novel class of FF Galilei-invariant advection–diffusion equations is introduced. This formulation combines the concept of Galilei invariance with FF operators, providing a new mathematical model for describing complex transport processes with memory and fractal characteristics.
- **Development of a numerical scheme based on FGFs:** A numerical scheme based on the FGFs is developed for solving the proposed model. The use of FGFs basis allows an efficient representation of the solution and provides a flexible framework for the numerical approximation of the governing equation.
- **Derivation of new integral operators:** New FF and integer-order integral operators associated with the FGFs are derived in the Atangana–Riemann–Liouville sense. These operators play a fundamental role in constructing the numerical procedure and enable the systematic treatment of the FF derivatives.
- **Transformation of the governing equation into an algebraic system:** By employing the derived operators within a collocation framework, the proposed method transforms the original FF partial differential equation into a solvable system of algebraic equations for the unknown coefficients.
- **Rigorous convergence analysis in Sobolev space:** A rigorous convergence analysis of the proposed method is carried out in the Sobolev space. The theoretical results provide error bounds for both the numerical approximation and the residual function, confirming the stability and reliability of the proposed scheme.

The structure of the current study is outlined as follows: In Section 2, some definitions and key concepts related to the FF calculus and the FGFs are summarized. Section 3 derives the FF and integer-order integral operators of the FGFs. Section 4 provides a numerical method for solving the FF nonlinear G-ID-DEs. Section 5 is devoted to the investigation of the convergence analysis of the proposed method in the Sobolev space. Section 6 presents the numerical examples along with the corresponding simulation results. A comprehensive conclusion is presented in Section 7.

2 Preliminaries

2.1 Fractal-fractional operator

Definition 1. *([33]). The one- and two-parameter Mittag–Leffler functions are defined, respectively, by*

$$E_{\varepsilon}(t) = \sum_{s=0}^{\infty} \frac{t^s}{\Gamma(s\varepsilon+1)}, \qquad \varepsilon \in R^+, t \in R, \tag{3}$$

and

$$E_{\varepsilon,\varsigma}(t) = \sum_{s=0}^{\infty} \frac{t^s}{\Gamma(s\varepsilon+\varsigma)}, \qquad \varepsilon,\varsigma \in R^+, t \in R.$$

Definition 2. *([26, 34]). Assume $\nu,\eta \in (0,1)$, and let $V(x,t)$ be a continuous real-valued function. The FF derivative of order (ν,η) in the ARL sense is formulated as:*

$${}^{ARL}D_t^{\nu,\eta}V(x,t) = \frac{M(\nu)}{1-\nu}\frac{d}{dt^{\eta}}\int_0^t E_\nu\left(\frac{-\nu(t-s)^\nu}{1-\nu}\right)V(x,s)ds,$$

where $M(\nu) = 1-\nu+\frac{\nu}{\Gamma(\nu)}$.

Definition 3. *([26, 34]). The FF integral $I_t^{\nu,\eta}$ of order (ν,η) in the ARL sense is defined as follows:*

$$I_t^{\nu,\eta}V(x,t) = \frac{\nu\eta}{M(\nu)\Gamma(\nu)}\int_0^t s^{\eta-1}V(x,s)(t-s)^{\nu-1}ds + \frac{\eta(1-\nu)t^{\eta-1}V(x,t)}{M(\nu)}. \tag{4}$$

The relation between the ARL FF derivative and the corresponding integral is given by [35]

$$(I_t^{\nu,\eta})({}^{ARL}D_t^{\nu,\eta})V(x,t) = V(x,t) - V(x,0), \qquad \nu,\eta \in (0,1). \tag{5}$$

Lemma 1. *([33]). Let $\nu,\eta \in (0,1)$ and $s \in N \cup \{0\}$. Thus, we find*

$${}^{ARL}D_t^{\nu,\eta}t^s = \frac{M(\nu)s!t^{s-\eta+1}}{\eta(1-\nu)}E_{\nu,s+1}\left(\frac{-\nu t^\nu}{1-\nu}\right).$$

2.2 Fractional-order Genocchi functions

In this subsection, the FGFs are briefly reviewed since they will be used as basis functions for constructing the numerical approximation in the proposed method. In particular, these functions provide an efficient tool for representing functions in the Hilbert spaces. The resulting expansions will later be employed in Section 3 to approximate the unknown solution and the related terms appearing in the considered model.

The FGFs defined on the interval $[0,1]$ are given by the following expression [25]:

$$G_i^\lambda(t) = \sum_{r=0}^{i}\binom{i}{r}g_{i-r}t^{r\lambda}, \qquad i = 1,2,\ldots, \tag{6}$$

where $g_i = 2B_i - 2^{i+1}B_i$ denotes the Genocchi numbers, B_i represents the well-known Bernoulli numbers and λ denotes the fractional order of the Genocchi polynomials, which is restricted to the interval $(0,1]$.

Additionally, these functions satisfy the following formula [25]:

$$\int_0^1 t^{\lambda-1}G_j^\lambda(t)G_i^\lambda(t)dt = \frac{2(-1)^j j!i!}{\lambda(j+i)!}g_{i+j}.$$

An arbitrary function $V(t)$ defined on the interval $L^2([0,1])$ can be represented using the FGFs in the following form:

$$V(t) = \sum_{i=1}^{\infty} b_i G_i^\lambda(t).$$

Accordingly, the following truncated series representation for $V(t)$ is considered:

$$V(t) \simeq \sum_{i=1}^{m} b_i G_i^{\lambda}(t) = B^T G_{\lambda}(t),$$

where

$$B = [b_1, b_2, \dots, b_m]^T, \qquad G_{\lambda}(t) = [G_1^{\lambda}(t), G_2^{\lambda}(t), \dots, G_m^{\lambda}(t)]^T.$$

The coefficient vector B is computed as follows:

$$B = D^{-1} Z,$$

where

$$D = < G_{\lambda}, G_{\lambda} > = \int_0^1 t^{\lambda-1} G_{\lambda}(t) G_{\lambda}^T(t) dt, \qquad Z = [z_1, z_2, \dots, z_m]^T,$$

and each component of Z is determined by the following expression:

$$z_i = < V, G_i^{\lambda} > = \int_0^1 t^{\lambda-1} V(t) G_i^{\lambda}(t) dt, \qquad i = 1, 2, \dots, m.$$

Similarly, any bivariate function $V(x,t)$ defined on $L^2([0,1] \times [0,1])$ can be approximated using the FGFs as follows:

$$V(x,t) \simeq \sum_{i=1}^{m_1} \sum_{j=1}^{m_2} u_{ij} G_i^{\lambda_1}(x) G_j^{\lambda_2}(t) = G_{\lambda_1}^T(x) U G_{\lambda_2}(t),$$

where $U = [u_{ij}]$ is a $m_1 \times m_2$ matrix.

Remark 1. *It should be noted that the matrix*

$$D = \langle G_{\lambda}, G_{\lambda} \rangle$$

is the Gram matrix associated with the FGFs basis functions under the weighted inner product

$$\langle f, g \rangle = \int_0^1 t^{\lambda-1} f(t) g(t)\, dt.$$

Since the functions $G_i^{\lambda}(t)$ are linearly independent and the weight function $t^{\lambda-1}$ is positive on $(0,1]$, the matrix D is positive definite and hence nonsingular. Consequently, the inverse matrix D^{-1} exists.

3 Formulated operators

In this section, we construct the FF and integer-order integral and derivative operators that we need in this work.

The FF integral operator in the ARL sense for the FGFs is expressed as:

$$I_t^{\nu,\eta} G_{\lambda_2}(t) = \Delta_1(t, \nu, \eta), \tag{7}$$

where $\Delta_1(t, \nu, \eta)$ is an $m_2 \times 1$ vector defined as:

$$\Delta_1(t, \nu, \eta) = [I_t^{\nu,\eta} G_1^{\lambda_2}(t), I_t^{\nu,\eta} G_2^{\lambda_2}(t), \dots, I_t^{\nu,\eta} G_{m_2}^{\lambda_2}(t)]^T,$$

where λ_2 represents the fractional order of the Genocchi polynomials associated with the variable t, and satisfies $\lambda_2 \in (0,1]$.
Using the definition of FGFs in Eq. (6) and the ARL integral in Eq. (4) for $1 \leq i \leq m_2$, we yield

$$I_t^{\nu,\eta} G_i^{\lambda_2}(t) = I_t^{\nu,\eta} \sum_{r=0}^{i} \binom{i}{r} g_{i-r} t^{r\lambda_2} = \sum_{r=0}^{i} \binom{i}{r} g_{i-r} I_t^{\nu,\eta} t^{r\lambda_2}. \tag{8}$$

For computing $I_t^{\nu,\eta} t^{r\lambda_2}$, we use the ARL integral in Eq. (4) as

$$\begin{aligned} I_t^{\nu,\eta}(t^{r\lambda_2}) &= \frac{\nu\eta}{M(\nu)} \int_0^t (t-s)^{\nu-1} s^{\eta-1} s^{r\lambda_2} ds + \frac{\eta(1-\nu)t^{\eta+r\lambda_2-1}}{M(\nu)} \\ &= \frac{\nu\eta}{M(\nu)} t^{\nu-1} * t^{\eta+r\lambda_2-1} + \frac{\eta(1-\nu)t^{\eta+r\lambda_2-1}}{M(\nu)}. \end{aligned} \tag{9}$$

By effecting the Laplace transform (ℓ) on relation (9), and then the inverse Laplace transform, we get

$$\ell(I_t^{\nu,\eta}(t^{r\lambda_2})) = \frac{\nu\eta\Gamma(\nu)\Gamma(\eta+r\lambda_2)}{M(\nu)s^{\nu+\eta+r\lambda_2}} + \frac{\eta(1-\nu)\Gamma(\eta+r\lambda_2)}{M(\nu)s^{\eta+r\lambda_2}}, \tag{10}$$

and

$$I_t^{\nu,\eta}(t^{r\lambda_2}) = \frac{\nu\eta\Gamma(\nu)\Gamma(\eta+r\lambda_2)}{M(\nu)\Gamma(\nu+\eta+r\lambda_2)} t^{\nu+\eta+r\lambda_2-1} + \frac{\eta(1-\nu)}{M(\nu)} t^{\eta+r\lambda_2-1}, \tag{11}$$

respectively. From Eqs. (8) and (11), we obtain

$$I_t^{\nu,\eta} G_i^{\lambda_2}(t) = \sum_{r=0}^{i} \binom{i}{r} g_{i-r} \left(\frac{\nu\eta\Gamma(\nu)\Gamma(\eta+r\lambda_2)}{M(\nu)\Gamma(\nu+\eta+r\lambda_2)} t^{\nu+\eta+r\lambda_2-1} + \frac{\eta(1-\nu)}{M(\nu)} t^{\eta+r\lambda_2-1} \right).$$

The integer-order integral operator of the second order associated with the FGFs is given by

$$I_x^2 G_{\lambda_1}(x) = \Delta_2(x,2), \tag{12}$$

where $\Delta_2(x,2)$ denotes an $m_1 \times 1$ vector given by

$$\Delta_2(x,2) = [I_x^2 G_1^{\lambda_1}(x), I_x^2 G_2^{\lambda_1}(x), \ldots, I_x^2 G_{m_1}^{\lambda_1}(x)]^T,$$

where λ_1 represents the fractional order of the Genocchi polynomials associated with the variable x, and satisfies $\lambda_1 \in (0,1]$.
Based on Eq. (6), the following result holds

$$\begin{aligned} I_x^2 G_i^{\lambda_1}(x) &= I_x^2 \sum_{r=0}^{i} \binom{i}{r} g_{i-r} x^{r\lambda_1} = \sum_{r=0}^{i} \binom{i}{r} g_{i-r} I_x^2 x^{r\lambda_1} \\ &= \sum_{r=0}^{i} \binom{i}{r} g_{i-r} \frac{x^{r\lambda_1+2}}{(r\lambda_1+1)(r\lambda_1+2)}. \end{aligned}$$

The integer-order integral operator of the one order $(\Delta_4(x,1))$ is obtained similarly to Eq. (12) as

$$I_x^1 G_{\lambda_1}(x) = \Delta_4(x,1). \tag{13}$$

Finally, we introduce the following operator:

$$\Delta_3(t,\nu,\eta) = D_t \Delta_1(t,\nu,\eta) = [D_t I_t^{\nu,\eta} G_1^{\lambda_2}(t), D_t I_t^{\nu,\eta} G_2^{\lambda_2}(t), \ldots, D_t I_t^{\nu,\eta} G_{m_2}^{\lambda_2}(t)]^T.$$

4 Description of computational approach

In this section, we propose a numerical method based on the FGFs and their operators to solve the FF G-ID-DE in (1)-(2).

For this aim, we approximate the function ${}^{ARL}D_t^{\nu,\eta}V_{xx}(x,t)$ using the FGFs, as follows:

$$ {}^{ARL}D_t^{\nu,\eta}V_{xx}(x,t) \simeq G_{\lambda_1}^T(x)UG_{\lambda_2}(t) = {}^{ARL}D_t^{\nu,\eta}V_{xx}^*(x,t). \tag{14} $$

Applying the operator $I_t^{\nu,\eta}$ to both sides of Eq. (14) and Eq. (5) we get

$$ V_{xx}(x,t) \simeq G_{\lambda_1}^T(x)UI_t^{\nu,\eta}G_{\lambda_2}(t) + V_{xx}(x,t)|_{t=0}. \tag{15} $$

From the FF integral operator in Eq. (7), along with the initial condition and Eq. (15), we yield

$$ V_{xx}(x,t) \simeq G_{\lambda_1}^T(x)U\Delta_1(t,\nu,\eta) + f''(x) = V_{xx}^*(x,t). \tag{16} $$

By performing a double integration of Eq. (16) with respect to x, we obtain:

$$ V(x,t) \simeq I_x^2 G_{\lambda_1}^T(x)U\Delta_1(t,\nu,\eta) + I_x^2 f''(x) + V(0,t) + x\frac{\partial}{\partial x}V(x,t)|_{x=0}. \tag{17} $$

Eq. (17) can be rewritten as follows:

$$ V(x,t) \simeq \Delta_2^T(x,2)U\Delta_1(t,\nu,\eta) + (f(x) - f(0) - xf'(0)) + g_0(t) + x\frac{\partial}{\partial x}V(x,t)|_{x=0}. \tag{18} $$

We substitute $x = 1$ into Eq. (18) to determine the unknown function $\frac{\partial}{\partial x}V(x,t)|_{x=0}$, as

$$ \frac{\partial}{\partial x}V(x,t)|_{x=0} = (g_1(t) - g_0(t)) - \Delta_2^T(1,2)U\Delta_1(t,\nu,\eta) - (f(1) - f(0) - f'(0)). \tag{19} $$

Adopting Eqs. (18)-(19), we achieve

$$ \begin{aligned} V(x,t) &\simeq \Delta_2^T(x,2)U\Delta_1(t,\nu,\eta) + (f(x) - f(0) - xf'(0)) + g_0(t) \\ &+ x((g_1(t) - g_0(t)) - \Delta_2^T(1,2)U\Delta_1(t,\nu,\eta) - (f(1) - f(0) - f'(0))) = V^*(x,t). \end{aligned} \tag{20} $$

The boundary conditions are exactly embedded in the trial approximation, ensuring that $V^*(0,t) = g_0(t)$ and $V^*(1,t) = g_1(t)$ are satisfied identically.
By differentiating Eq. (20) with respect to the variables t and x, respectively, we conclude

$$ \begin{aligned} V_t(x,t) &\simeq \Delta_2^T(x,2)U\Delta_3(t,\nu,\eta) + g_0'(t) \\ &+ x((g_1'(t) - g_0'(t)) - \Delta_2^T(1,2)U\Delta_3(t,\nu,\eta)) = V_t^*(x,t), \end{aligned} \tag{21} $$

and

$$ \begin{aligned} V_x(x,t) \simeq\ & \Delta_4^T(x,1)U\Delta_1(t,\nu,\eta) + (f'(x) - f'(0)) \\ & + ((g_1(t) - g_0(t)) - \Delta_2^T(1,2)U\Delta_1(t,\nu,\eta) - (f(1) - f(0) - f'(0))) = V_x^*(x,t). \end{aligned} \tag{22} $$

Substituting Eqs. (14), (16), (20), (21), and (22) in Eq. (1), we obtain the residual function

$$R(x,t) = V_t^*(x,t) + \rho V_x^*(x,t) - \iota^{ARL}D_t^{\nu,\eta} V_{xx}^*(x,t) - \mathscr{H}(x,t,V^*(x,t)) - K(x,t). \tag{23}$$

Ultimately, the use of Legendre nodes in Eq. (23) yields the following system of algebraic equations, where the source term $K(x,t)$ is assumed to be evaluated exactly at the collocation points (x_i,t_j) (i.e., $K^*(x_i,t_j) = K(x_i,t_j)$):

$$R(x_i,t_j) = 0, \qquad i = 1,2,\ldots,m_1; j = 1,2,\ldots,m_2. \tag{24}$$

Here, the collocation points are selected as the roots of the shifted Legendre polynomials. Specifically, the spatial collocation points x_i, $i = 1,2,\ldots,m_1$, are chosen as the roots of

$$P_{m_1}(x_i) = 0,$$

and the temporal collocation points t_j, $j = 1,2,\ldots,m_2$, are chosen as the roots of

$$P_{m_2}(t_j) = 0.$$

Hence, there are m_1 collocation points in the spatial direction and m_2 collocation points in the temporal direction. Since these roots lie strictly inside the interval $(0,1)$, the boundary points are not included among the collocation nodes. This is justified by the fact that the boundary conditions are exactly satisfied by the trial approximation (20), and therefore only interior collocation points are needed.

The nonlinear algebraic system obtained from the collocation discretization was solved by Newton's iterative method using FindRoot in Mathematica 14. The unknown coefficients were initialized by the zero vector. The built-in automatic Jacobian approximation was used, and the default values of AccuracyGoal, PrecisionGoal, and MaxIterations were retained. Hence, the stopping criterion and derivative evaluation were handled internally by Mathematica. For all examples, the Newton iteration converged rapidly (typically within 5–10 iterations), and the residual norm at the final solution was less than 10^{-12} indicating that no convergence difficulties were encountered.

Remark 2. *In the proposed formulation, the invertibility of U is not required. The matrix U acts as an unknown coefficient matrix whose entries are determined by solving the resulting nonlinear algebraic system via Newton's iterative method. Consequently, no invertibility assumptions on U are imposed. As noted by Stoer and Bulirsch [43], the efficiency of Newton-type methods heavily depends on the quality of the initial approximation. For simplicity and consistency, a zero vector is chosen as the initial guess for all unknown coefficients in the numerical simulations. Employing this systematic choice yields stable convergence to the numerical solution using Mathematica, thereby ensuring the stability of the Newton iteration and enhancing the reproducibility of the presented results.*

5 Convergence analysis

This section analyzes the convergence of the proposed method in Section 4 for solving the FF nonlinear G-ID-DE in (1)-(2). In this part, we consider $\lambda_1 = \lambda_2 = \lambda$ and $m_1 = m_2 = m$.

The Sobolev norm over the domain $\Omega = (0,1)^d$ in $\mathbb{R}^d$, where $d = 2,3$ and $\alpha \geq 2$, is defined as follows [29]:

$$\| V \|_{H^{\alpha}(\Omega)} = \left(\sum_{j=0}^{\alpha} \sum_{i=1}^{d} \| D_i^{(j)} V \|_{L^2(\Omega)}^2 \right)^{\frac{1}{2}}, \tag{25}$$

where $D_i^{(j)}$ shows the jth derivative of V with respect to the ith variable. The notation $|V|_{H^{\alpha;m}(\Omega)}$ is defined as follows:

$$|V|_{H^{\alpha;m}(\Omega)} = \left(\sum_{j=\min(\alpha,m+1)}^{\alpha} \sum_{i=1}^{d} \| D_i^{(j)} V \|_{L^2(\Omega)}^2 \right)^{\frac{1}{2}}.$$

Theorem 1. *Let $V \in H^{\alpha}(\Omega)$ with $\alpha \geq 1$, and $V^*(x,t)$ is the best approximation of $V(x,t)$, then we have*

$$\| V - V^* \|_{L^2(\Omega)} \leq c\lambda^{1-\alpha} m^{1-\alpha} |V|_{H^{\alpha;m\lambda}(\Omega)}, \tag{26}$$

for $1 \leq \zeta \leq \alpha$

$$\| V - V^* \|_{H^{\zeta}(\Omega)} \leq c\lambda^{\theta(\zeta)-\alpha} m^{\theta(\zeta)-\alpha} |V|_{H^{\alpha;m\lambda}(\Omega)}, \tag{27}$$

where c depends on α and

$$\theta(\zeta) = \begin{cases} 0, & \zeta = 0, \\ 2\zeta - \frac{1}{2}, & \zeta > 0. \end{cases}$$

Proof. The proof is similar to the proof of Theorem 5.1 in [29]. □

Lemma 2. *Assume $V \in H^{\alpha}(\Omega)$ with $\alpha \geq 1$, and $d \geq 2$, then we get*

$$\| V_t - V_t^* \|_{L^2(\Omega)} \leq c\lambda^{\theta(\zeta)-\alpha} m^{\theta(\zeta)-\alpha} |V|_{H^{\alpha;m\lambda}(\Omega)}, \tag{28}$$

$$\| V_x - V_x^* \|_{L^2(\Omega)} \leq c\lambda^{\theta(\zeta)-\alpha} m^{\theta(\zeta)-\alpha} |V|_{H^{\alpha;m\lambda}(\Omega)}, \tag{29}$$

$$\| V_{xx} - V_{xx}^* \|_{L^2(\Omega)} \leq c\lambda^{\theta(\zeta)-\alpha} m^{\theta(\zeta)-\alpha} |V|_{H^{\alpha;m\lambda}(\Omega)}. \tag{30}$$

Proof. According to the definition of the Sobolev norm in Eq. (25) for $d \geq 2$, we have

$$\| V_t - V_t^* \|_{L^2(\Omega)} \leq \| V - V^* \|_{H^{\zeta}(\Omega)},$$

From Eq. (27), we yields

$$\| V_t - V_t^* \|_{L^2(\Omega)} \leq c\lambda^{\theta(\zeta)-\alpha} m^{\theta(\zeta)-\alpha} |V|_{H^{\alpha;m\lambda}(\Omega)}.$$

Relations (29) and (30) are obtained in a similar way. □

Theorem 2. *([34]). Suppose $D_t^{i\lambda} V \in C(0,1]$ holds for $i = 0,1,\ldots,m$. If V^* represents the best approximation to V, then we obtain*

$$\| {}^{ARL}D_t^{\nu,\eta} V - {}^{ARL}D_t^{\nu,\eta} V^* \|_{L^2(\Omega)} \leq \delta \| V - V^* \|_{L^2(\Omega)}. \tag{31}$$

Lemma 3. *Let $D_t^{i\lambda} V_{xx} \in C(0,1]$ for $i = 0,1,\ldots,m$, and $V \in H^{\alpha}(\Omega)$ for $\alpha \geq 2$. Then we conclude*

$$\| {}^{ARL}D_t^{\nu,\eta} V_{xx} - {}^{ARL}D_t^{\nu,\eta} V_{xx}^* \|_{L^2(\Omega)} \leq \delta c\lambda^{\theta(\zeta)-\alpha} m^{\theta(\zeta)-\alpha} |V|_{H^{\alpha;m\lambda}(\Omega)}. \tag{32}$$

Proof. Using Theorem 2 and Eq. (30), we get

$$\| D_t^{\nu,\eta} V_{xx} - D_t^{\nu,\eta} V_{xx}^* \|_{L^2(\Omega)} \leq \delta \| V_{xx} - V_{xx}^* \|_{L^2(\Omega)} \leq \delta c \lambda^{\theta(\zeta)-\alpha} m^{\theta(\zeta)-\alpha} |V|_{H^{\alpha;m\lambda}(\Omega)}. \quad (33)$$

□

Theorem 3. *Assume that the conditions of Theorem 1, and Lemmas 2-3 are satisfied, and that $\mathscr{H}$ satisfies the Lipschitz condition with the Lipschitz constant Ξ. Then we have*

$$\begin{aligned} \| R \|_{L^2(\Omega)} &\leq (1+\rho+\iota\delta) c \lambda^{\theta(\zeta)-\alpha} m^{\theta(\zeta)-\alpha} |V|_{H^{\alpha;m\lambda}(\Omega)} \\ &+ \Xi c \lambda^{1-\alpha} m^{1-\alpha} |V|_{H^{\alpha;m\lambda}(\Omega)}, \end{aligned}$$

where R is the residual error function defined in (23).

Proof. Using Eqs. (1) and (23), and considering that the source term $K(x,t)$ is evaluated exactly (which leads to its cancellation in the subtraction), we derive

$$\begin{aligned} R(x,t) &= V_t^*(x,t) + \rho V_x^*(x,t) - \iota^{ARL} D_t^{\nu,\eta} V_{xx}^*(x,t) - \mathscr{H}(x,t,V^*(x,t)) \\ &- V_t(x,t) - \rho V_x(x,t) + \iota^{ARL} D_t^{\nu,\eta} V_{xx}(x,t) + \mathscr{H}(x,t,V(x,t)). \end{aligned}$$

It follows that

$$\begin{aligned} \| R \|_{L^2(\Omega)} &\leq \| V_t - V_t^* \|_{L^2(\Omega)} + \rho \| V_x - V_x^* \|_{L^2(\Omega)} \\ &+ \iota \| {}^{ARL}D_t^{\nu,\eta} V_{xx} - {}^{ARL}D_t^{\nu,\eta} V_{xx}^* \|_{L^2(\Omega)} + \Xi \| V - V^* \|_{L^2(\Omega)}. \end{aligned}$$

Finally, by employing Eqs. (26), (28), (29) and (31), we derive the upper bound for $\| R \|_{L^2(\Omega)}$ as follows:

$$\begin{aligned} \| R \|_{L^2(\Omega)} &\leq (1+\rho+\iota\delta) c \lambda^{\theta(\zeta)-\alpha} m^{\theta(\zeta)-\alpha} |V|_{H^{\alpha;m\lambda}(\Omega)} \\ &+ \Xi c \lambda^{1-\alpha} m^{1-\alpha} |V|_{H^{\alpha;m\lambda}(\Omega)}. \end{aligned}$$

This concludes the proof. □

Remark 3. *Therefore, the proposed scheme converges with rate $O(\lambda^{1-\alpha} m^{1-\alpha})$ in $L^2(\Omega)$ and $O(\lambda^{\theta(\zeta)-\alpha} m^{\theta(\zeta)-\alpha})$ in $H^\zeta(\Omega)$. Moreover, from Theorem 3 the residual error satisfies*

$$\| R \|_{L^2(\Omega)} = O(\max\{\lambda^{1-\alpha} m^{1-\alpha}, \lambda^{\theta(\zeta)-\alpha} m^{\theta(\zeta)-\alpha}\}),$$

which also characterizes the convergence rate of the residual of the proposed scheme.

Remark 4. *This convergence analysis is primarily tailored to the specific model investigated in this study. In addition to the smoothness of the exact solution and the approximation properties of the basis functions, the mathematical structure of the equation is a key factor. Specifically, Theorem 3 shows that the final error estimate depends on the Lipschitz continuity of the nonlinear term $\mathscr{H}$. Therefore, the convergence is guaranteed under these model-specific assumptions and cannot be generalized to state that any arbitrary operator with first-order temporal and spatial derivatives, and second-order spatial derivatives, will necessarily meet the convergence conditions.*

Remark 5. *The mathematical convergence of the approximation and the proposed numerical scheme is established in Theorems 1 and 3, respectively. In addition, the numerical results in Tables 3 and 5 confirm this convergence behavior.*

6 Numerical results

This section presents the numerical validation of the mentioned method. It demonstrates that our approach is effective for FF nonlinear G-ID-DE. The computations associated with the examples were performed using Mathematical 14. Also, we report the CPU time (seconds) in the examples, which have been obtained on a 2.4 GHz Core i7 personal computer with 16 GB of RAM.

Example 1. Consider the following FF nonlinear G-ID-DE:

$$V_t(x,t)+V_x(x,t) = {}^{ARL}D_t^{\nu,\eta}V_{xx}(x,t)+\sin(x)V^2(x,t)+\sin(x)+(t+1)\cos(x)-(t+1)^2\sin^3(x) + \sin(x)[\frac{M(\nu)t^{2-\eta}}{\eta(1-\nu)}E_{\nu,2}(\frac{-\nu t^{\nu}}{1-\nu})+\frac{M(\nu)t^{1-\eta}}{\eta(1-\nu)}E_{\nu,1}(\frac{-\nu t^{\nu}}{1-\nu})],$$

so that

$$V(x,0)=\sin(x), \quad V(0,t)=0, \quad V(1,t)=(t+1)\sin(1).$$

The exact solution corresponding to this problem is $V(x,t)=(t+1)\sin(x)$.

Table 1 reports the absolute errors (AEs) with $\nu=\eta=0.99, m_1=3, m_2=2$ and different values of λ_1 and λ_2. The AEs corresponding to $\lambda_1=\frac{2}{3}, \lambda_2=\frac{1}{2}, m_1=3, m_2=2$ and diverse values of ν,η are provided in Table 2. In addition, the maximum absolute errors (MAEs) over all collocation points is also reported in Tables 1 and 2 in order to illustrate the global accuracy of the proposed scheme. To illustrate the computational efficiency of the proposed method, the CPU execution times for $\lambda_1=\frac{2}{3}, \lambda_2=\frac{1}{2}, \nu=0.99, \eta=0.6$ with different values of m_1 and m_2 are reported in the Table 3. The behavior of numerical results (NRs) and AEs for $\nu=\eta=0.99, \lambda_1=\frac{2}{3}, \lambda_2=\frac{1}{2}$, $m_1=3$ and $m_2=2$ are shown in Figure 1, while Figure 2 displays the NRs for $\nu=\eta=0.5$. Moreover, the sensitivity of the solution $V(0.25,t)$ to different fractional orders $\nu,\eta=0.6,0.7,0.8,0.9$ with $m_1=3$ and $m_2=2$ is demonstrated in Figure 3.

Table 1: The AEs and MAEs with $\nu=\eta=0.99$, for Example 1

(x,t)	$\lambda_1=\lambda_2=\frac{1}{5}$	$\lambda_1=\lambda_2=\frac{1}{2}$	$\lambda_1=\lambda_2=\frac{2}{3}$	$\lambda_1=\lambda_2=\frac{5}{6}$	$\lambda_1=\lambda_2=1$
$(0.1,0.1)$	3.34×10^{-3}	2.07×10^{-4}	1.82×10^{-4}	3.49×10^{-4}	4.29×10^{-4}
$(0.2,0.2)$	1.00×10^{-2}	9.55×10^{-4}	3.48×10^{-4}	9.37×10^{-4}	1.23×10^{-3}
$(0.3,0.3)$	1.77×10^{-2}	2.12×10^{-3}	4.23×10^{-4}	1.64×10^{-3}	2.29×10^{-3}
$(0.4,0.4)$	2.50×10^{-2}	3.55×10^{-3}	3.58×10^{-4}	2.35×10^{-3}	3.47×10^{-3}
$(0.5,0.5)$	3.06×10^{-2}	5.04×10^{-3}	1.51×10^{-4}	2.95×10^{-3}	4.62×10^{-3}
$(0.6,0.6)$	3.35×10^{-2}	6.26×10^{-3}	1.46×10^{-4}	3.34×10^{-3}	5.54×10^{-3}
$(0.7,0.7)$	3.28×10^{-2}	6.84×10^{-3}	4.38×10^{-4}	3.40×10^{-3}	5.97×10^{-3}
$(0.8,0.8)$	2.75×10^{-2}	6.33×10^{-3}	5.96×10^{-4}	3.02×10^{-3}	5.53×10^{-3}
$(0.9,0.9)$	1.68×10^{-2}	4.22×10^{-3}	4.87×10^{-4}	1.97×10^{-3}	3.76×10^{-3}
MAEs	3.89×10^{-2}	6.84×10^{-3}	5.96×10^{-4}	9.86×10^{-3}	9.47×10^{-3}

Table 2: The AEs and MAEs with $\lambda_1 = \frac{2}{3}, \lambda_2 = \frac{1}{2}$, for Example 1

(x,t)	$\nu = 0.99$			$\eta = 0.99$		
	$\eta = 0.2$	$\eta = 0.4$	$\eta = 0.6$	$\nu = 0.2$	$\nu = 0.4$	$\nu = 0.6$
$(0.1, 0.1)$	6.80×10^{-3}	5.17×10^{-4}	4.69×10^{-4}	2.81×10^{-3}	5.42×10^{-3}	7.85×10^{-3}
$(0.2, 0.2)$	1.30×10^{-2}	9.89×10^{-4}	9.13×10^{-4}	1.00×10^{-2}	1.35×10^{-2}	1.73×10^{-2}
$(0.3, 0.3)$	1.82×10^{-2}	1.40×10^{-3}	1.18×10^{-3}	1.93×10^{-2}	2.24×10^{-2}	2.65×10^{-2}
$(0.4, 0.4)$	2.22×10^{-2}	1.79×10^{-3}	1.21×10^{-3}	2.89×10^{-2}	3.07×10^{-2}	3.44×10^{-2}
$(0.5, 0.5)$	2.47×10^{-2}	2.18×10^{-3}	1.01×10^{-3}	3.73×10^{-2}	3.72×10^{-2}	3.98×10^{-2}
$(0.6, 0.6)$	2.53×10^{-2}	2.50×10^{-3}	6.50×10^{-4}	4.26×10^{-2}	4.06×10^{-2}	4.18×10^{-2}
$(0.7, 0.7)$	2.38×10^{-2}	2.64×10^{-3}	2.31×10^{-4}	4.33×10^{-2}	3.99×10^{-2}	3.96×10^{-2}
$(0.8, 0.8)$	1.94×10^{-2}	2.41×10^{-3}	1.06×10^{-4}	3.76×10^{-2}	3.37×10^{-2}	3.24×10^{-2}
$(0.9, 0.9)$	1.17×10^{-2}	1.60×10^{-3}	2.21×10^{-4}	2.38×10^{-2}	2.08×10^{-2}	1.94×10^{-2}
MAEs	2.70×10^{-2}	3.93×10^{-3}	7.45×10^{-3}	5.64×10^{-2}	4.86×10^{-2}	4.44×10^{-2}

Table 3: The AEs and CPU times with $\lambda_1 = \frac{2}{3}, \lambda_2 = \frac{1}{2}, \nu = 0.99, \eta = 0.6$ for Example 1

(x,t)	$m_2 = 1$			$m_2 = 2$		
	$m_1 = 2$	$m_1 = 4$	$m_1 = 6$	$m_1 = 1$	$m_1 = 2$	$m_1 = 3$
$(0.1, 0.1)$	3.68×10^{-3}	1.73×10^{-3}	1.80×10^{-3}	1.46×10^{-3}	6.51×10^{-4}	4.69×10^{-4}
$(0.2, 0.2)$	9.33×10^{-3}	3.25×10^{-3}	3.46×10^{-3}	3.45×10^{-3}	1.53×10^{-3}	9.13×10^{-4}
$(0.3, 0.3)$	1.52×10^{-2}	3.71×10^{-3}	4.09×10^{-3}	4.92×10^{-3}	2.46×10^{-3}	1.18×10^{-3}
$(0.4, 0.4)$	2.02×10^{-2}	2.95×10^{-3}	3.49×10^{-3}	5.33×10^{-3}	3.29×10^{-3}	1.21×10^{-3}
$(0.5, 0.5)$	2.35×10^{-2}	1.15×10^{-3}	1.84×10^{-3}	4.53×10^{-3}	3.91×10^{-3}	1.01×10^{-3}
$(0.6, 0.6)$	2.45×10^{-2}	1.21×10^{-3}	4.43×10^{-4}	2.73×10^{-3}	4.22×10^{-3}	6.50×10^{-4}
$(0.7, 0.7)$	2.28×10^{-2}	3.45×10^{-3}	2.69×10^{-3}	4.38×10^{-4}	4.10×10^{-3}	2.31×10^{-4}
$(0.8, 0.8)$	1.82×10^{-2}	4.69×10^{-3}	4.04×10^{-3}	1.52×10^{-3}	3.47×10^{-3}	1.06×10^{-4}
$(0.9, 0.9)$	1.06×10^{-2}	4.69×10^{-3}	3.52×10^{-3}	2.09×10^{-3}	2.16×10^{-3}	2.21×10^{-4}
CPU	0.062	0.078	0.078	0.047	0.047	0.062

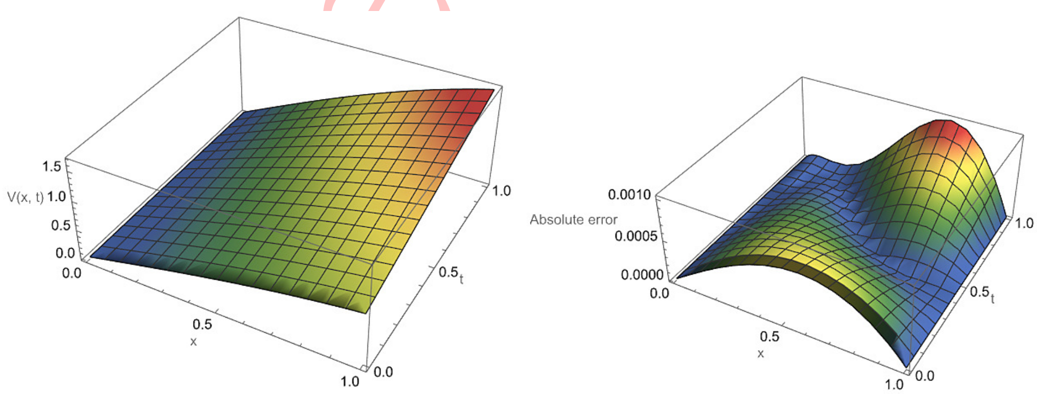

Figure 1: The NRs and AEs for $\nu = \eta = 0.99, \lambda_1 = \frac{2}{3}, \lambda_2 = \frac{1}{2}$, for Example 1

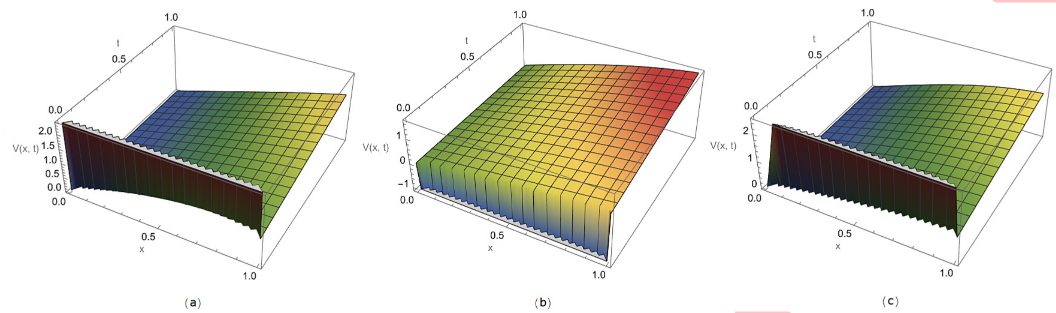

Figure 2: The NRs for $(a): \lambda_1 = \lambda_2 = \frac{1}{5}, (b): \lambda_1 = \lambda_2 = \frac{2}{3}, (c): \lambda_1 = \lambda_2 = 1$ with $\nu = \eta = 0.5$, for Example 1

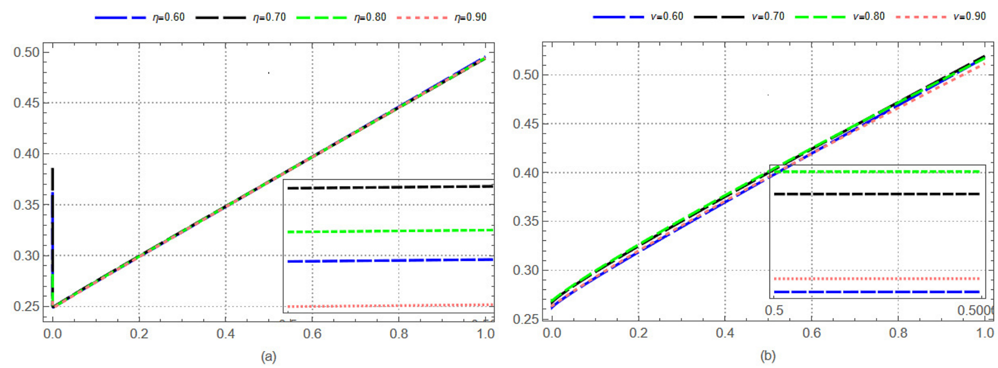

Figure 3: The $V(0.25,t)$ for $(a): \nu = 0.99, (b): \eta = 0.99$, for Example 1

Example 2. Consider the following FF nonlinear G-ID-DE:

$$V_t(x,t) + 2V_x(x,t) = \frac{3}{2}{}^{ARL}D_t^{\nu,\eta} V_{xx}(x,t) + e^{-V^2(x,t)} + 2te^x + 2t^2e^x$$
$$-e^{-t^4e^{2x}} - 3\frac{e^x M(\nu) t^{3-\eta}}{\eta(1-\nu)} E_{\nu,3}\left(\frac{-\nu t^\nu}{1-\nu}\right),$$

so that

$$V(x,0) = 0, \quad V(0,t) = t^2, \quad V(1,t) = t^2 e.$$

The exact solution corresponding to this problem is $V(x,t) = t^2 e^x$.

Table 4 presents the AEs for $\lambda_1 = \lambda_2 = 1, m_1 = 1, m_2 = 2$ with various values of ν, η. The NRs and AEs corresponding to $\nu = \eta = 0.99, m_1 = 1, m_2 = 2$ and $\lambda_1 = \lambda_2 = \frac{1}{2}, \frac{2}{3}, 1$ are reported in Table 5. In addition, the MAEs over all collocation points is also reported in Tables 4 and 5 in order to illustrate the global accuracy of the proposed scheme. To illustrate the computational efficiency of the proposed method, the CPU execution times for $\lambda_1 = \lambda_2 = 1, \nu = 0.99$ with different values of m_1 and m_2 are reported in the Table 6. Furthermore, to demonstrate the systematic convergence of the scheme, the numerical convergence rates (denoted by R) have been computed and added to Table 6. The 3D graphs of the NRs and AEs for $\nu = \eta = 0.99, 0.55$ with $\lambda_1 = \lambda_2 = 1$ and $m_1 = 1, m_2 = 2$ are plotted and shown in Figure 4. Figure 5 illustrates the behavior of $V(0.25,t)$ for $m_1 = 1, m_2 = 2$ with different values of ν, η.

Table 4: The AEs and MAEs with $\lambda_1 = \lambda_2 = 1$, for Example 2

(x,t)	$\nu=\eta=0.5$	$\nu=\eta=0.6$	$\nu=\eta=0.7$	$\nu=\eta=0.8$	$\nu=\eta=0.9$	$\nu=\eta=1$
$(0.1,0.1)$	6.72×10^{-2}	3.44×10^{-2}	1.76×10^{-2}	8.42×10^{-3}	2.81×10^{-3}	6.60×10^{-5}
$(0.2,0.2)$	7.23×10^{-2}	3.78×10^{-2}	1.99×10^{-2}	1.01×10^{-2}	3.89×10^{-3}	1.29×10^{-4}
$(0.3,0.3)$	5.77×10^{-2}	2.85×10^{-2}	1.40×10^{-2}	6.95×10^{-3}	2.94×10^{-3}	5.09×10^{-4}
$(0.4,0.4)$	3.67×10^{-2}	1.46×10^{-2}	5.02×10^{-3}	1.83×10^{-3}	1.11×10^{-3}	5.52×10^{-4}
$(0.5,0.5)$	1.76×10^{-2}	2.37×10^{-3}	2.80×10^{-3}	2.58×10^{-3}	1.99×10^{-4}	3.75×10^{-4}
$(0.6,0.6)$	5.19×10^{-3}	4.48×10^{-3}	6.52×10^{-3}	4.22×10^{-3}	1.31×10^{-4}	2.66×10^{-3}
$(0.7,0.7)$	1.16×10^{-3}	4.64×10^{-3}	5.11×10^{-3}	2.32×10^{-3}	2.42×10^{-3}	6.02×10^{-3}
$(0.8,0.8)$	3.57×10^{-3}	2.02×10^{-4}	2.40×10^{-5}	1.98×10^{-3}	5.60×10^{-3}	9.09×10^{-3}
$(0.9,0.9)$	6.61×10^{-3}	4.85×10^{-3}	4.44×10^{-3}	5.04×10^{-3}	6.68×10^{-3}	8.84×10^{-3}
MAEs	7.33×10^{-2}	8.56×10^{-2}	3.60×10^{-2}	1.37×10^{-2}	6.68×10^{-3}	9.84×10^{-3}

Table 5: The NRs, AEs and MAEs with $\nu = \eta = 0.99$, for Example 2

(x,t)	$\lambda_1=\lambda_2=\frac{1}{2}$		$\lambda_1=\lambda_2=\frac{2}{3}$		$\lambda_1=\lambda_2=1$	
	NR	*AE*	*NR*	*AE*	*NR*	*AE*
$(0.1,0.1)$	0.014093	3.04×10^{-3}	0.012825	1.77×10^{-3}	0.011118	6.60×10^{-5}
$(0.2,0.2)$	0.054855	5.99×10^{-3}	0.052285	3.42×10^{-3}	0.048727	1.29×10^{-4}
$(0.3,0.3)$	0.128308	6.82×10^{-3}	0.125192	3.70×10^{-3}	0.120978	5.09×10^{-4}
$(0.4,0.4)$	0.244806	6.11×10^{-3}	0.241842	3.15×10^{-3}	0.238140	5.52×10^{-4}
$(0.5,0.5)$	0.417494	5.31×10^{-3}	0.415087	2.91×10^{-3}	0.412555	3.75×10^{-4}
$(0.6,0.6)$	0.661678	5.72×10^{-3}	0.659927	3.96×10^{-3}	0.658618	2.66×10^{-3}
$(0.7,0.7)$	0.994470	7.73×10^{-3}	0.993254	6.52×10^{-3}	0.992759	6.02×10^{-3}
$(0.8,0.8)$	1.434560	1.02×10^{-3}	1.433690	9.35×10^{-3}	1.433430	9.09×10^{-3}
$(0.9,0.9)$	2.002040	9.75×10^{-3}	2.001460	9.18×10^{-3}	2.001110	8.84×10^{-3}
MAEs	1.02×10^{-2}		9.35×10^{-3}		9.09×10^{-3}	

Example 3. Consider the following FF nonlinear G-ID-DE:

$$V_t(x,t) + V_x(x,t) = {}^{ARL}D_t^{\nu,\eta} V_{xx}(x,t) + V^2(x,t) + \beta t^{\beta-1}\cos(x) - t^{\beta}\sin(x)$$
$$+\cos(x)\frac{M(\nu)\beta! t^{\beta-\eta+1}}{\eta(1-\nu)} E_{\nu,\beta+1}\left(\frac{-\nu t^{\nu}}{1-\nu}\right) - t^{2\beta}\cos^2(x),$$

so that

$$V(x,0) = 0, \quad V(0,t) = t^{\beta}, \quad V(1,t) = t^{\beta}\cos(1),$$

where $0 < \beta < 1$, and The exact solution corresponding to this problem is $V(x,t) = t^{\beta}\cos(x)$.

Table 6: The AEs and CPU times with $\lambda_1 = \lambda_2 = 1, \nu = \eta = 0.99$ for Example 2

(x,t)	$m_2 = 1$			$m_2 = 2$	
	$m_1 = 1$	$m_1 = 2$	$m_1 = 3$	$m_1 = 1$	$m_1 = 2$
$(0.1, 0.1)$	7.73×10^{-3}	6.49×10^{-3}	5.84×10^{-3}	6.60×10^{-5}	6.93×10^{-5}
$(0.2, 0.2)$	2.33×10^{-2}	2.02×10^{-2}	1.77×10^{-2}	1.29×10^{-4}	7.76×10^{-5}
$(0.3, 0.3)$	3.92×10^{-2}	3.59×10^{-2}	2.99×10^{-2}	5.09×10^{-4}	1.24×10^{-4}
$(0.4, 0.4)$	5.01×10^{-2}	4.87×10^{-2}	3.82×10^{-2}	5.52×10^{-4}	5.76×10^{-4}
$(0.5, 0.5)$	5.23×10^{-2}	5.54×10^{-2}	3.99×10^{-2}	3.75×10^{-4}	1.19×10^{-3}
$(0.6, 0.6)$	4.49×10^{-2}	5.38×10^{-2}	3.40×10^{-2}	2.66×10^{-3}	1.74×10^{-3}
$(0.7, 0.7)$	2.93×10^{-2}	4.39×10^{-2}	2.16×10^{-2}	6.02×10^{-3}	1.96×10^{-3}
$(0.8, 0.8)$	1.03×10^{-2}	2.77×10^{-2}	6.70×10^{-3}	9.09×10^{-3}	1.65×10^{-3}
$(0.9, 0.9)$	3.71×10^{-3}	1.03×10^{-2}	4.02×10^{-3}	8.84×10^{-3}	8.15×10^{-4}
CPU	0.109	0.110	0.141	0.047	0.110
R	–	0.25259	0.23563	–	2.21343

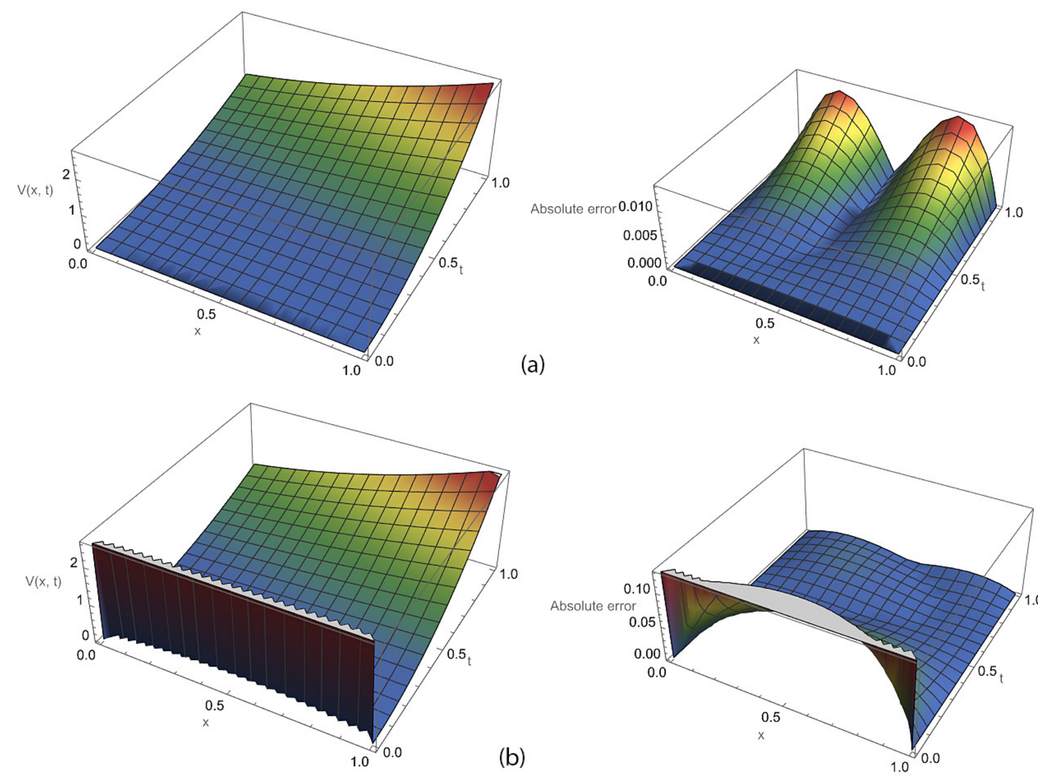

Figure 4: The NRs and AEs for $(a): \nu = \eta = 0.99, (b): \nu = \eta = 0.55$, with $\lambda_1 = \lambda_2 = 1$ for Example 2

Table 7 presents the NRs, AEs, MAEs and CPU times in seconds for $\nu = \eta = 0.99, \lambda_1 = \frac{2}{3}, \lambda_2 = \frac{1}{2}$ with $m_1 = 3, m_2 = 2$ across various choices of β. Figure 6 displays the 3D plots of the NRs and AEs for $m_1 = 3, m_2 = 2$, with $\lambda_1 = \frac{2}{3}, \lambda_2 = \frac{1}{2}$.

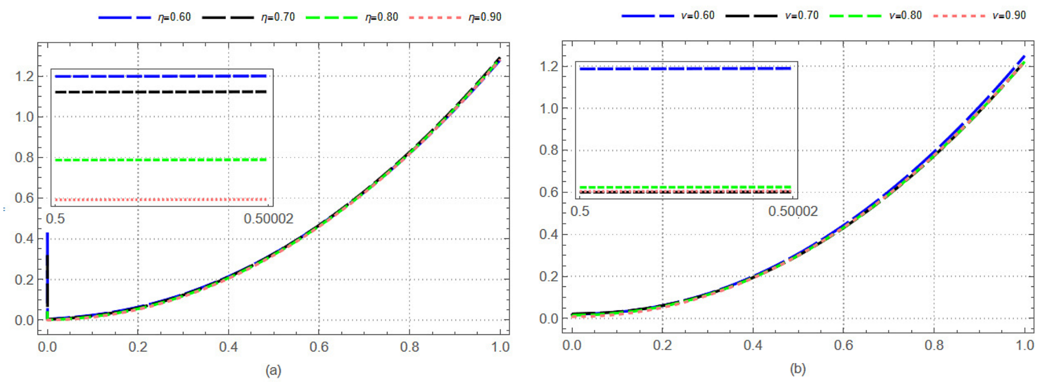

Figure 5: The $V(0.25,t)$ for $(a): \nu = 0.99, (b): \eta = 0.99$, for Example 2

Table 7: The NRs, AEs, MAEs and CPU times with $\nu = \eta = 0.99, \lambda_1 = \frac{2}{3}, \lambda_2 = \frac{1}{2}$ for Example 3

(x,t)	$\beta = 0.4$		$\beta = 0.5$		$\beta = 0.6$	
	NR	*AE*	*NR*	*AE*	*NR*	*AE*
$(0.1,0.1)$	0.387182	8.94×10^{-3}	0.309289	5.36×10^{-3}	0.247114	2.82×10^{-3}
$(0.2,0.2)$	0.499503	1.53×10^{-2}	0.429545	8.75×10^{-3}	0.369077	4.06×10^{-3}
$(0.3,0.3)$	0.572457	1.78×10^{-2}	0.514212	9.05×10^{-3}	0.460955	2.95×10^{-3}
$(0.4,0.4)$	0.621220	1.72×10^{-2}	0.575392	7.14×10^{-3}	0.531295	2.30×10^{-4}
$(0.5,0.5)$	0.650259	1.48×10^{-2}	0.616465	4.08×10^{-3}	0.582151	3.16×10^{-4}
$(0.6,0.6)$	0.661267	1.15×10^{-2}	0.638470	8.32×10^{-4}	0.613774	6.31×10^{-3}
$(0.7,0.7)$	0.655084	8.07×10^{-3}	0.641702	1.79×10^{-3}	0.625839	8.35×10^{-3}
$(0.8,0.8)$	0.632352	4.86×10^{-3}	0.626278	3.12×10^{-3}	0.617876	8.47×10^{-3}
$(0.9,0.9)$	0.593790	2.17×10^{-4}	0.592368	2.66×10^{-3}	0.589462	5.93×10^{-3}
MAE	1.78×10^{-2}		9.13×10^{-3}		7.66×10^{-3}	
CPU	0.125		0.078		0.141	

Remark 6. *In Example 3, the exact solution is $V(x,t) = t^{\beta}\cos(x)$ with $0 < \beta < 1$, so*

$$V_t(x,t) = \beta t^{\beta-1}\cos(x),$$

which is singular as $t \to 0^+$. This endpoint singularity reduces the temporal regularity of the solution and explains the relatively larger errors observed for smaller β. Since the proposed method uses smooth global basis functions, its approximation efficiency near $t = 0t = 0$ may deteriorate in such cases. A singularity-adapted basis or graded/adaptive refinement near the initial time may improve the accuracy.

7 Conclusions

This study introduced a novel class of FF differential equations, namely the FF G-ID-DEs, which encapsulates complex dynamic behaviors governed by memory and non-locality. To address the challenges associated with solving this new class of equations, a robust numerical framework based on the FGFs has

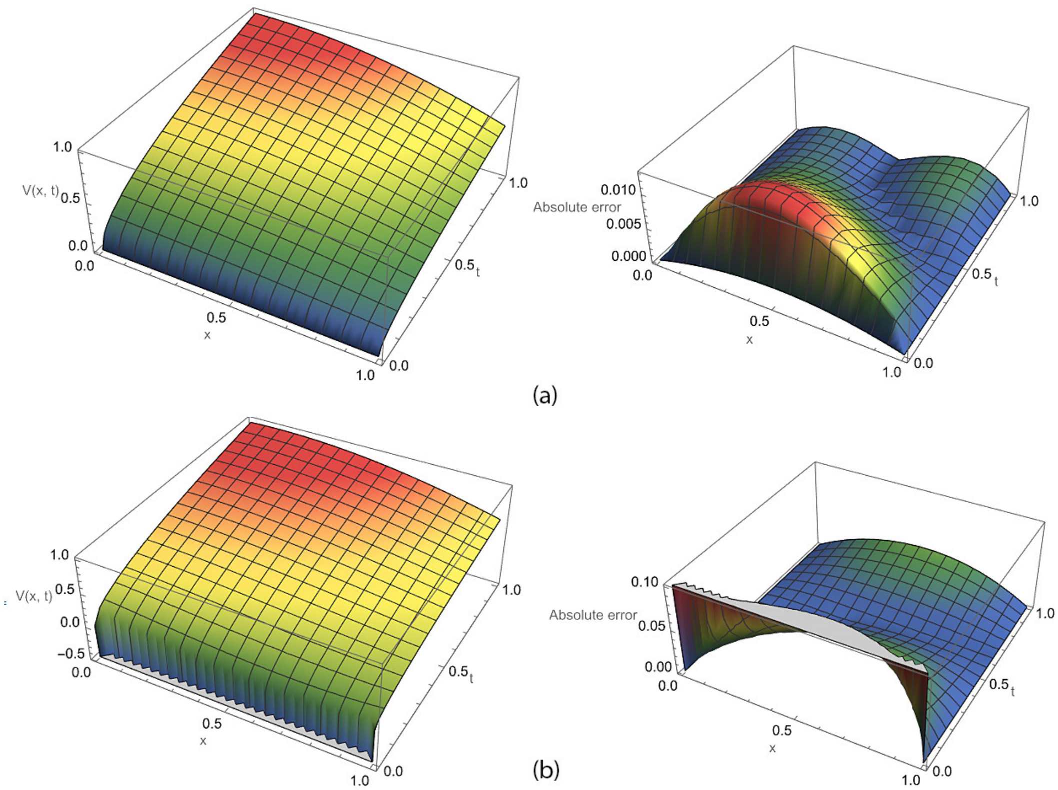

Figure 6: The NRs and AEs for $(a): \nu = \eta = 0.99, (b): \nu = \eta = 0.55$, with $\beta = \frac{1}{2}, \lambda_1 = \frac{2}{3}, \lambda_2 = \frac{1}{2}$ for Example 3

been developed. By deriving the integral and derivative operators of the FGFs within the ARL context, and employing their analytical properties within a collocation scheme, the original problem is successfully transformed into a tractable system of algebraic equations. The proposed methodology not only ensures numerical feasibility but also exhibits strong convergence toward the exact solution. Theoretical analysis is supported by illustrative examples, which confirm the accuracy and practical relevance of the approach. Overall, the framework presented herein provides a promising foundation for further exploration of FF models and their applications in various fields of science and engineering. Future research directions motivated by the present study can be outlined as follows:

- Extending the numerical framework to handle singularly perturbed regimes where spatial and temporal diffusion parameters become arbitrarily small. This involves developing parameter-uniform schemes and layer-resolving meshes to address the sharp boundary layers and high gradients typical in fluid dynamics applications.
- Extending the proposed method to variable-order and distributed-order G-ID-DEs.
- Developing parallel algorithms and high-performance computing–based implementations to significantly enhance the scalability of the proposed method for solving large-scale three-dimensional problems.
- Combining the proposed methodology with deep optimization techniques, such as reinforcement

learning, to handle dynamic or time-dependent fractional optimal control problems and further enhance adaptability in complex environments.
- Extending the proposed framework to problems with Neumann, Robin, and mixed boundary conditions.
- Developing singularity-adapted basis functions and graded or adaptive refinement strategies for solutions with endpoint singularities.

Author Contributions

All authors contributed equally to this work.

Funding

The authors received no financial support for the research, authorship, and publication of this paper.

Availability of supporting data

Data will be made available on reasonable request.

Declaration

The authors declare no competing interests.

Acknowledgments

We express our sincere thanks to the anonymous referees for their valuable suggestions that improved the final manuscript.

References

[1] M. Abbaszadeh, M. Dehghan, *The Crank-Nicolson/interpolating stabilized element-free Galerkin method to investigate the fractional Galilei invariant advection-diffusion equation*, Math. Methods Appl. Sci. **44(4)** (2021) 2752-68.

[2] K.A. Abro, A. Atangana, *A comparative study of convective fluid motion in rotating cavity via Atangana–Baleanu and Caputo–Fabrizio fractal–fractional differentiations*, Eur. Phys. J. Plus. **135(2)** (2020) 1-6.

[3] A. Atangana, *Fractal-fractional differentiation and integration: connecting fractal calculus and fractional calculus to predict complex system*, Chaos Solit. Fractals **102** (2017) 396-406.

[4] A. Atangana, S. Qureshi, *Modeling attractors of chaotic dynamical systems with fractal–fractional operators*, Chaos Solit. Fractals **123** (2019) 320-37.

[5] C.M. Chen, F. Liu, V. Anh, I. Turner, *Numerical simulation for the variable-order Galilei invariant advection diffusion equation with a nonlinear source term*, Appl. Math. Comput. **217(12)** (2011) 5729-42.

[6] G. Dewangan, A. Singh, A. Kanaujiya, *Generalized distributed-order fractional optimal control problem using Laguerre wavelet method*, J. Math. Model. **13(4)** (2025) 747-65.

[7] N. Engheta, *On fractional calculus and fractional multipoles in electromagnetism*, IEEE Trans. Antennas Propag. **44(4)** (1996) 554-66.

[8] S. Eslami, M. Ilati, M. Dehghan, *A local meshless method for solving multi-dimensional Galilei invariant fractional advection-diffusion equation*, Eng. Anal. Bound. Elem. **143** (2022) 283-92.

[9] B. Ghosh, J. Mohapatra, *An adaptive scheme based on the cubic B-Spline collocation technique for time-fractional singular parabolic problems with semilinearity*, J. Comput. Nonlinear Dyn. **20(7)** (2025) 071006.

[10] B. Ghosh, J. Mohapatra, *Improved layer-adaptive computational approaches for solving mildly singular delayed time-fractional parabolic problems*, J. Appl. Math. Comput. **71(6)** (2025) 8689-714.

[11] B. Ghosh, J. Mohapatra, P. Das, *Nonlocal convergence analysis of a layer-adaptive ADI scheme for 2D semilinear reaction-subdiffusion equations involving singularity*. Math. Comput. Simul. **248** (2026) 421-439.

[12] M.H. Heydari, A. Atangana, Z. Avazzadeh, *Numerical solution of nonlinear fractal-fractional optimal control problems by Legendre polynomials*, Math. Methods Appl. Sci. **44(4)** (2021) 2952-63.

[13] M.H. Heydari, A. Atangana, Z. Avazzadeh, M.R. Mahmoudi, *An operational matrix method for nonlinear variable-order time fractional reaction–diffusion equation involving Mittag-Leffler kernel*, Eur. Phys. J. Plus. **135(2)** (2020) 1-9.

[14] M.H. Heydari, M. Razzaghi, *A hybrid method based on the Chebyshev cardinal functions/wavelets for time fractional coupled Klein–Gordon–Schrödinger equations*, J. Comput. Appl. Math. **427** (2023) 115142.

[15] M.H. Heydari, M. Razzaghi, D. Baleanu, *Orthonormal piecewise Vieta-Lucas functions for the numerical solution of the one-and two-dimensional piecewise fractional Galilei invariant advection-diffusion equations*, J. Adv. Res. **49** (2022) 175.

[16] M. Hosseininia, M.H. Heydari, Z. Avazzadeh, *The numerical treatment of nonlinear fractal–fractional 2D Emden–Fowler equation utilizing 2D Chelyshkov polynomials*, Fractals **28(08)** (2020) 2040042.

[17] M. Hosseininia, M.H. Heydari, F.M. Ghaini, Z. Avazzadeh, *A meshless technique based on the moving least squares shape functions for nonlinear fractal-fractional advection-diffusion equation*, Eng. Anal. Bound. Elem. **127** (2021) 8-17.

[18] V.V. Kulish, J.L. Lage, *Application of fractional calculus to fluid mechanics*. J. Fluids Eng. **124(3)** (2002) 803-6.

[19] S. Kumar, P. Das, *Analysis of an efficient parameter uniform domain decomposition approach for singularly perturbed gierer-meinhardt type nonlinear coupled systems of parabolic problems*, Int. J. Numer. Anal. **22(4)** (2025) 459-82.

[20] S. Kumar, R I, P. Das, *Impact of mixed boundary conditions and nonsmooth data on layer-originated nonpremixed combustion problems: Higher-order convergence analysis*, Stud. Appl. Math. **153(4)** (2024) e12763.

[21] S. Kumar, P. Das, *Second-order a priori and a posteriori error estimations for integral boundary value problems of nonlinear singularly perturbed parameterized form*, Numer. Algorithms **99(3)** (2025) 1365-92.

[22] S. Kumar, P. Pandey, S. Das, *Gegenbauer wavelet operational matrix method for solving variable-order non-linear reaction–diffusion and Galilei invariant advection–diffusion equations*, Comput. Appl. Math. **38(4)** (2019) N-PAG.

[23] H.T. Ngo, T.N. Vo TN, M. Razzaghi, *An effective method for solving nonlinear fractional differential equations*. Eng. Comput. **38(Suppl 1)** (2022) 207-18.

[24] A. Patawari, S. Kumar, P. Das, *A modified iterative PINN algorithm for strongly coupled system of boundary layer originated convection diffusion reaction problems in MHD flows with analysis*, Netw. Heterog. Media. **20(3)** (2025) 1026-60.

[25] P. Rahimkhani, *Numerical solution of nonlinear stochastic differential equations with fractional Brownian motion using fractional-order Genocchi deep neural networks*, Commun. Nonlinear Sci. Numer. Simul. **126** (2023) 107466.

[26] P. Rahimkhani, M.H. Heydari, *Fractional shifted Morgan–Voyce neural networks for solving fractal-fractional pantograph differential equations*, Chaos, Solit. Fractals **175** (2023) 114070.

[27] P. Rahimkhani, M.H. Heydari, *Numerical investigation of ψ-fractional differential equations using wavelets neural networks*, Comput. Appl. Math. **44(2)** (2025) 54.

[28] P. Rahimkhani, Y. Ordokhani, *A computational method based on Legendre wavelets for solving distributed order fractional diffrential equations*, J. Math. Model. **9(3)** (2021) 501-516

[29] P. Rahimkhani, Y. Ordokhani, *Generalized fractional-order Bernoulli–Legendre functions: an effective tool for solving two-dimensional fractional optimal control problems*, IMA J. Math. Control Inf. **36(1)** (2019) 185-212.

[30] P. Rahimkhani, Y. Ordokhani, M. Razzaghi, *Fractional-order clique functions to solve left-sided Bessel fractional integro-differential equations*, Chaos Solit. Fractals **192** (2025) 116025.

[31] P. Rahimkhani, Y. Ordokhani, S. Sabermahani, *Hahn hybrid functions for solving distributed order fractional Black-Scholes European option pricing problem arising in financial market*, Math. Methods Appl. Sci. **46(6)** (2023) 6558-77.

[32] P. Rahimkhani, S. Sedaghat, *Alternative wavelets for the solution of variable-order fractal-fractional differential equations system with power and Mittag-Leffler kernels*, J. Appl. Anal. Comput. **15** (2025) 1830-61.

[33] P. Rahimkhani, S. Sedaghat, Y. Ordokhani, *An effective computational solver for fractal-fractional 2D integro-differential equations*, J. Appl. Math. Comput. **70(4)** (2024) 3411-40.

[34] A. Rayal, S.R. Verma, *Numerical analysis of pantograph differential equation of the stretched type associated with fractal-fractional derivatives via fractional order Legendre wavelets*, Chaos, Solitons Fractals. **139** (2020) 110076.

[35] A. Rayal, S.R. Verma, *Two-dimensional Gegenbauer wavelets for the numerical solution of tempered fractional model of the nonlinear Klein-Gordon equation*, Appl. Numer. Math. **174** (2022) 191-220.

[36] A. Rezazadeh, Z. Avazzadeh, *Numerical approach for solving two dimensional fractal-fractional PDEs using peridynamic method*, Int. J. Comput. Math. **99(3)** (2022) 486-505.

[37] Y.A. Sabawi, S. Santra, P. Das, N.A. Mohammad, *H^1 stability and convergence analysis of the L1/L1-2 Legendre spectral method for non-local weakly singular integro-PDEs*, Calcolo **62(4)** (2025) 1-46.

[38] S. Sabermahani, Y. Ordokhani, P. Rahimkhani, *Application of generalized Lucas wavelet method for solving nonlinear fractal-fractional optimal control problems*, Chaos Solit. Fractals **170** (2023) 113348.

[39] S. Saini, P. Das, S. Kumar, *Computational cost reduction for coupled system of multiple scale reaction diffusion problems with mixed type boundary conditions having boundary layers*, Revista de la Real Academia de Ciencias Exactas, Físicas y Naturales. Serie A. Matemáticas **117(2)** (2023) 66.

[40] S. Saini, P. Das, S. Kumar, *Parameter uniform higher order numerical treatment for singularly perturbed Robin type parabolic reaction diffusion multiple scale problems with large delay in time*, Appl. Numer. Math. **196** (2024) 1-21.

[41] S. Santra, J. Mohapatra, P. Das, D. Choudhuri, *Higher order approximations for fractional order integro-parabolic partial differential equations on an adaptive mesh with error analysis*, Comput. Math. Appl. **150** (2023) 87-101.

[42] H.M. Srivastava, K.M. Saad, *Numerical simulation of the fractal-fractional Ebola virus*, Fractal Fract. **4(4)** (2020) 49.

[43] J. Stoer, R. Bulirsch, *Topics in integration*, in Introduction to Numerical Analysis (pp. 117-158), New York, NY: Springer New York, 2002.

[44] Y.Q. Wei, D.Y. Liu, D. Boutat, *Innovative fractional derivative estimation of the pseudo-state for a class of fractional order linear systems*, Automatica, **99** (2019) 157-66.

[45] X.J. Yang, F. Gao, Y. Ju, *General Fractional Derivatives with Applications in Viscoelasticity*, Academic Press; 2020.

[46] M.A. Zaky, D. Baleanu, J.F. Alzaidy, E. Hashemizadeh, *Operational matrix approach for solving the variable-order nonlinear Galilei invariant advection–diffusion equation*, Adv. Differ. Equ. **2018(1)** (2018) 102.